SERMeQ model produces realistic retreat of 155 Greenland outlet glaciers

Lizz Ultee[1,1] and Jeremy N. Bassis[2,2]

[1]Massachusetts Institute of Technology
[2]University of Michigan-Ann Arbor

November 30, 2022

Abstract

The rate of land ice loss due to iceberg calving is a key source of variability among model projections of 21st century sea-level rise. It is especially challenging to account for mass loss due to iceberg calving in Greenland, where ice drains to the ocean through hundreds of outlet glaciers, many smaller than typical model grid scale. Here, we apply a numerically efficient network flowline model (SERMeQ) forced by surface mass balance to simulate an upper bound on decadal calving retreat of 155 grounded outlet glaciers of the Greenland Ice Sheet—resolving five times as many outlets as was previously possible. We show that the upper bound holds for 91\% of glaciers examined and that simulated changes in terminus position correlate with observed changes. SERMeQ can provide a physically consistent constraint on forward projections of the dynamic mass loss from the Greenland Ice Sheet associated with different climate projections.

SERMeQ model produces a realistic upper bound on calving retreat for 155 Greenland outlet glaciers

Lizz Ultee[1], Jeremy N. Bassis[2]

[1]Department of Earth, Atmospheric, and Planetary Sciences, Massachusetts Institute of Technology, Cambridge, MA, 02139

[2]Department of Climate & Space Sciences, University of Michigan, Ann Arbor, MI 48109

Key Points:

- We tested an upper-bound model of calving retreat of 155 ocean-terminating outlet glaciers that drain the Greenland Ice Sheet.
- Our physics-based method produces terminus positions that correlate with observed positions for 103 glaciers without model tuning.
- Our model bounds retreat rates on 91% of glaciers tested, providing a constraint for future sea level projections.

Corresponding author: Lizz Ultee, `ehultee@umich.edu`

Abstract

The rate of land ice loss due to iceberg calving is a key source of variability among model projections of 21st century sea-level rise. It is especially challenging to account for mass loss due to iceberg calving in Greenland, where ice drains to the ocean through hundreds of outlet glaciers, many smaller than typical model grid scale. Here, we apply a numerically efficient network flowline model (SERMeQ) forced by surface mass balance to simulate an upper bound on decadal calving retreat of 155 grounded outlet glaciers of the Greenland Ice Sheet—resolving five times as many outlets as was previously possible. We show that the upper bound holds for 91% of glaciers examined and that simulated changes in terminus position correlate with observed changes. SERMeQ can provide a physically consistent constraint on forward projections of the dynamic mass loss from the Greenland Ice Sheet associated with different climate projections.

1 Introduction

The Greenland Ice Sheet is currently the largest single contributor to global mean sea level rise (van den Broeke et al., 2017). It discharges ice mass to the ocean through three main processes: release of surface meltwater, submarine melting where ice is in contact with the ocean, and the detachment (calving) of icebergs. The ice mass lost to submarine melting has only recently been directly observed (Sutherland et al., 2019) and remains difficult to estimate for the whole ice sheet (Beckmann et al., 2018), but it is clear that enhanced surface melting and calving processes have resulted in increased mass discharge since the late 1990s (van den Broeke et al., 2016; Enderlin et al., 2014; Khan et al., 2014).

Processes that control surface melt are increasingly resolved in regional models (Mottram et al., 2017; Noël et al., 2018). Iceberg calving, by contrast, remains poorly understood, with multiple contradictory parameterizations incorporated into ice sheet/glacier models (Benn, Cowton, et al., 2017; Morlighem et al., 2016; Levermann et al., 2012). Furthermore, iceberg calving can remove mass more rapidly than is possible through melting alone, contributing to rapid tidewater glacier retreat through mechanisms like tidewater glacier instability (Meier & Post, 1987) and the recently-described Marine Ice Cliff Instability (Bassis & Walker, 2012; Pollard et al., 2015).

Simulating discharge from the Greenland Ice Sheet is further complicated by the local factors affecting ice discharge at the nearly 200 outlet glaciers that connect the ice sheet to the ocean (e.g. Catania et al., 2018; Enderlin et al., 2018). For all but the largest outlets, iceberg calving occurs at smaller scales than are captured in continental-scale ice sheet models. Existing estimates of dynamic mass loss from Greenland outlets have come from extrapolating perturbations on the largest outlets (Price et al., 2011; Nick et al., 2013), simulating the sea level contribution from only selected outlets (Choi et al., 2017; Morlighem et al., 2019), or simulating the entire ice sheet at a spatial resolution of 500 m (Aschwanden et al., 2016, 2019) to resolve about 30 of the nearly 200 glaciers that drain the Greenland Ice Sheet.

Despite these achievements, more than 100 outlet glaciers, responsible for $\sim 1/3$ of current Greenland Ice Sheet discharge (Enderlin et al., 2014), are not routinely simulated, and their dynamics cannot necessarily be inferred from the dynamics of larger outlets. Another layer of spatial complexity arises in that many outlet glaciers collect ice from several interacting tributary branches that are themselves also smaller than typical ice sheet model grid scale. The small scale of tributary glacier networks feeding outlets makes them especially challenging to simulate in continental ice sheet models, requiring model resolution of hundreds to tens of meters to adequately resolve.

A more fundamental challenge in projecting mass loss due to calving is the incompatibility of fracture-driven iceberg calving with the assumption of continuum deforma-

tion inherent in most ice sheet models (e.g. Price et al., 2015; Winkelmann et al., 2011; Greve, 2000). Simple empirical parameterizations can relate calving rate to continuous variables, such as proglacial water depth (Brown et al., 1982; Hanson & Hooke, 2000), but may not hold into the future as climate forcing enters a new statistical regime. Physically-based calving laws, such as the fracture field approach developed by Albrecht and Levermann (2012) or von Mises calving law developed for Greenland by Morlighem et al. (2016), often impose an empirically-adjustable calving rate parameter. Recent work has sought to simulate ice failure using continuum damage mechanics, with some success in a variety of case studies (Borstad et al., 2012; Duddu et al., 2013; Krug et al., 2014; Sun et al., 2017; Mercenier et al., 2019). However, at present the evolution of the damage field through a damage production function is also empirical, with multiple tuned parameters that are poorly constrained by laboratory or field measurements (Emetc et al., 2018). Another recent approach couples a granular model that allows true fracture and calving to a finite-element model that solves an approximation to the Stokes equations for viscous deformation, offering a very promising basis for process-scale simulation of fully-dynamic calving (Benn, Åström, et al., 2017). Unfortunately, the coupled approach remains too computationally expensive for century-scale projections. Despite their promise, neither continuum damage models nor granular calving models have been able to reproduce observed multi-annual evolution of calving front positions in Greenland.

Improving projections of 21st-century sea level rise requires models that can *(i)* reproduce complex patterns of glacier advance and retreat currently observed in Greenland and *(ii)* efficiently simulate dynamic discharge and iceberg calving from individual outlet glaciers for a spectrum of climate scenarios. To address this, we have developed a simple model to simulate advance, retreat, and dynamic mass loss due to calving on networks of marine-terminating glaciers (Ultee & Bassis, 2016, 2017; Bassis & Ultee, 2019). Our model framework, called SERMeQ, is able to directly simulate decade-to-century-scale evolution of hundreds of outlet glaciers in response to surface mass balance forcing across multiple climate scenarios. This explicit simulation capability, together with recent observations of more than 200 Greenland outlet glacier termini (Joughin et al., 2015, updated 2017a), makes it possible to evaluate our model's performance in a wide range of glacier environments. Here, we show that SERMeQ bounds retreat rates, and reproduces patterns of present-day observed changes in terminus position of 155 Greenland outlet glaciers, providing one of the largest validations of any calving parameterization. On the basis of this validation, our model physics can be incorporated into global glacier and ice sheet models to compute a physically-consistent upper constraint on the century-scale glaciological contribution to global sea level rise.

2 Methods

2.1 SERMeQ ice dynamics model

SERMeQ—the Simple Estimator of Retreat Magnitude and ice flux (Q), *sermeq* meaning "glacier" in Greenlandic—is a width-averaged, vertically-integrated model that determines centerline glacier surface elevation corresponding to a given terminus position. The ice dynamics are based on a perfectly-plastic limiting case of a viscoplastic rheology (Nye, 1951; Bassis & Ultee, 2019), with modifications to allow calving at a grounded ice-water interface (Ultee & Bassis, 2016) and interaction between multiple tributary glaciers (Ultee & Bassis, 2017). Our flowline-modeling approach is compatible with other flowline-based models such as the Open Global Glacier Model (Maussion et al., 2019), but SER-MeQ focuses specifically on near-terminus dynamics of marine glaciers to simulate the calving process.

Rather than imposing an empirical calving rate, SERMeQ self-consistently calculates the maximum rate of terminus advance or retreat at each time step for a given climate forcing. Terminus position evolves in response to near-terminus stretching, bedrock

topography, and changes in catchment-wide surface mass balance as described in Ultee (2018) and Bassis and Ultee (2019),

$$\frac{dL}{dt} = \frac{\dot{a} - H\frac{\partial U}{\partial x} - U\frac{\partial H}{\partial x}}{\frac{\partial H_y}{\partial x} - \frac{\partial H}{\partial x}} \ . \tag{1}$$

In Equation 1, $H = H(x,t)$ is the ice thickness, $U = U(x,t)$ the ice velocity, $\dot{a} = \dot{a}(x,t)$ the net ice accumulation rate, H_y the thickness at which effective stress within the ice reaches its yield strength (Equation S1), and all terms are evaluated at the instantaneous terminus position, $x = L(t)$ (see Supplementary Text S1-2). For a change in terminus position determined from Equation 1, SERMeQ calculates a new steady-state glacier surface elevation profile and calculates change in glacier volume above buoyancy (Supplementary Figure S1). The latter produces a net contribution to global mean sea level (example in Supplementary Text S1, not evaluated in this validation exercise).

The only adjustable model parameters are ice temperature T, which is used to calculate the horizontal stretching rate $\partial U/\partial x$ at the terminus, and yield strength τ_y, which is used to calculate the yield thickness H_y (Supplementary Text S1-S3). Both are material quantities that can be independently constrained by laboratory and field measurements. Crucially, we do not tune either of our parameters to match changes in terminus position. Comparison of simulated with observed terminus position thus provides a completely independent validation.

Here, we extend the physical realism and applicability of our model to demonstrate that it can simulate calving retreat of a wide variety of marine-terminating glaciers. Novel elements of SERMeQ specific to this application include upstream forcing with surface mass balance from a regional climate model (Mottram et al., 2018) and the automatic selection of networks of flowlines with varying width (traced from Joughin et al., 2015, updated 2017b, see Supplementary Text S5).

2.2 Identification of flowline networks

We first identified 181 Greenland outlet glaciers that have multiple terminus positions recorded in Joughin et al. (2015, updated 2017a). For each glacier, we then defined a network of interacting flowlines with spatially variable width by tracing ice surface velocity from Joughin et al. (2015, updated 2017b, and see Supplementary Text S5). We extracted ice surface and bed elevation from BedMachine version 3 (Morlighem et al., 2017) and applied a Gaussian filter to produce width-averaged topography. Where the data suggested the presence of short, transient ice tongues, we removed the floating portion from consideration and simulated the grounding line as the "terminus". We removed three glaciers with long, persistent ice tongues, as SERMeQ is unable to simulate ice tongue evolution. Thirteen of the 181 outlets had initial termini grounded above sea level and iceberg calving is thus unlikely to dominate dynamic mass changes there. We removed those thirteen glaciers from consideration as well. Noisy or missing data that produced unphysical bed topography caused us to remove ten additional outlets, leaving 155 glaciers for our analysis.

For the remaining 155 outlet glaciers, we defined the initial terminus as the grounded-ice point along our central flowline that lies closest to the centroid of the 2006 terminus reported in Joughin et al. (2015, updated 2017a). We optimized a single parameter, the yield strength of ice, to best fit the 2006 observed surface profile, as described in Ultee and Bassis (2017). We used a best-guess ice temperature T of $-10°$ C for all glaciers. We then found the catchment-wide, annual mean surface mass balance forcing for each outlet, $\dot{a}$ in Equation 1, from HIRHAM regional climate model reanalysis (Mottram et al., 2018; Rae et al., 2012; Lucas-Picher et al., 2012), and simulated resulting changes between 2006 and 2014 in ice extent (Figures 1-3) and volume above buoyancy (Figure 4 and Supplementary Figure 1). Finally, we compared the simulated changes in termi-

nus position with observed changes reported in Joughin et al. (2015, updated 2017a) for the same period. Because our optimization of τ_y considers only the initial observed surface profile, and the changes in terminus position are an independent response to changes in surface mass balance, this comparison examines an independent model prediction that is not tuned to match observations.

2.3 Comparison with observations

We extracted all available terminus position records from (Joughin et al., 2015, updated 2017a) for each year within our simulated period: 2006, 2007, 2009, 2013, and 2014. Each terminus position record consists of one or more points; records with multiple points trace across-flow variation in terminus position. We projected all available points from a given record onto the central flowline of the corresponding glacier network, and we identified the space between the most seaward and most landward points of that projection as the "observational range". We also tracked the change over time in the position of the terminus centroid projected on the flowline, which we identified as the "observed (terminus-centroid) retreat rate". Finally, we compared the simulated retreat rates with the observed terminus-centroid retreat rates (Figure 2) and the simulated terminus positions with the observational range (Figures 3-4a).

3 Results

3.1 An upper bound on calving retreat for 155 Greenland outlets

Figure 1 shows the total retreat we simulated for each glacier between 2006 and 2014, arranged by approximate outlet position. SERMeQ simulates less than 5 km of length change during the observed period on most outlets. There is no relationship between outlet glacier latitude and magnitude of upper-bound retreat: simulated glacier response to downscaled climate reanalysis forcing is not a simple function of annual average temperature. Dynamic glacier response depends on glacier geometry, as previous studies have also highlighted (Felikson et al., 2017; Benn, Cowton, et al., 2017; Catania et al., 2018).

Equation 1 includes an assumption that the glacier calving front is a yield surface, which produces a theoretical upper bound on calving retreat for a given glacier geometry and surface mass balance (see Bassis & Ultee, 2019). Thus, provided there are no significant errors in the bed geometry and surface mass balance used, we anticipate that SERMeQ-simulated rates of retreat will generally overestimate observed rates. Figure 2 shows that SERMeQ satisfies this expectation and overestimates retreat for 91% (108/119) of glaciers for which more than two terminus position observations are available to constrain the observed retreat rate.

The bulk model results shown in Figures 1 and 2 summarize multi-annual change in terminus position simulated across Greenland. Figure 3 compares observed and simulated terminus position change for example glaciers where SERMeQ underestimates, overestimates, or correctly captures the observed rate of retreat. Apuseeq Anittangasikkaajuk, which is 2 km wide at the terminus and has a small floating ice tongue, is one of a handful of outlets where SERMeQ underestimates observed retreat (Fig. 3a). The simulated terminus positions are still within the (small) observational range in that case. SERMeQ strongly overestimates retreat of Helheim Glacier, a large and high-flux glacier on Greenland's east coast whose terminus approaches flotation (Fig. 3b). On Sermeq Kujalleq (Danish: Jakobshavn Isbræ), a very large and well-studied outlet glacier on the southwest coast of Greenland, the simulated retreat of 6 km is comparable to observed retreat (Fig. 3c).
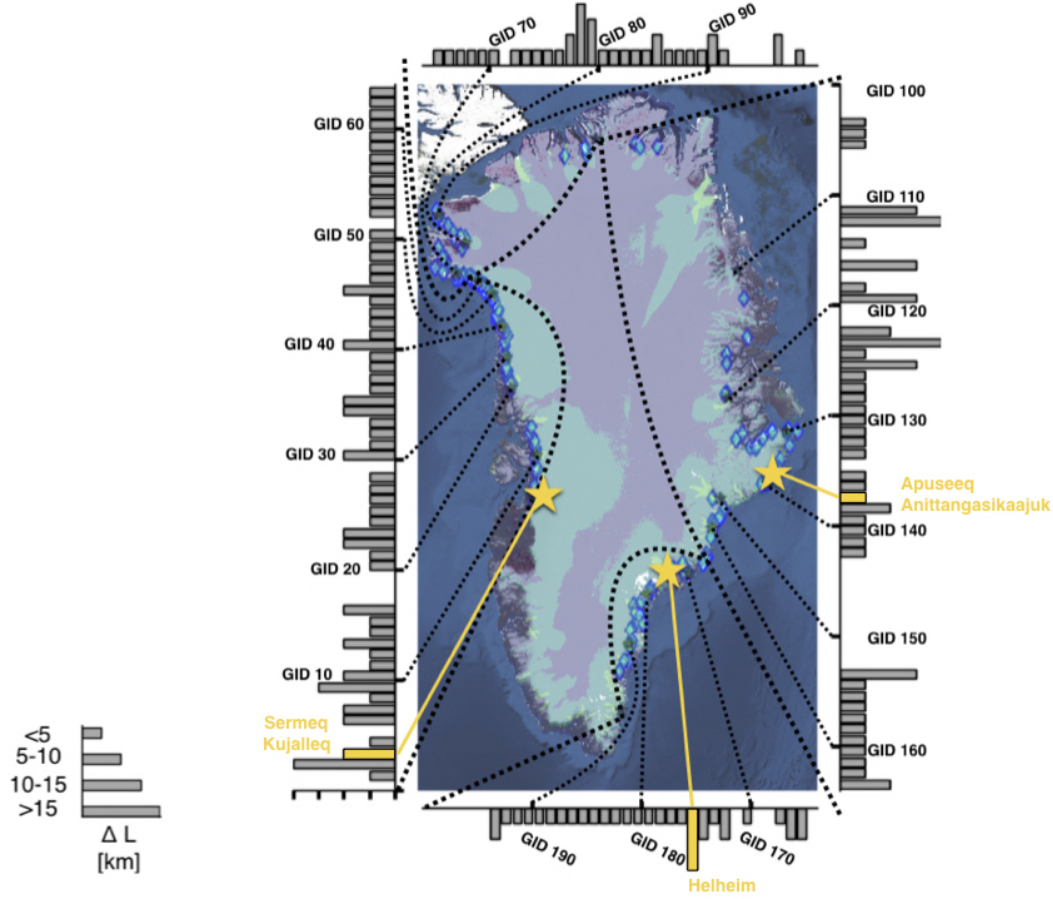
Figure 1. Map view of the 2006-2014 retreat simulated in this work. Bars indicate magnitude of simulated retreat for each glacier, with glaciers identified and ordered by their MEaSUREs outlet glacier ID number (1-200). Glacier ID 1, which is in the Disko Bay region, appears in the lower left; glacier IDs increase clockwise around the map border. Blue diamonds mark the map location of each outlet we simulated, and every 10th glacier ID is labelled and connected to its outlet location in black. A table of MEaSUREs glacier IDs and names appears in the Supplementary Material. Border spaces with no bar correspond to outlets where data was not sufficient to initialize a SERMeQ simulation, or where our analysis indicated SERMeQ would not be applicable (see Section 2). Yellow bars and map stars show the case-study glaciers highlighted in Figure 3. Coloured overlay on the satellite map is ice velocity derived from Sentinel-1 observations (ENVEO, 2017), shown on a logarithmic scale such that fast-moving outlet networks appear brighter than slow-moving inland ice.
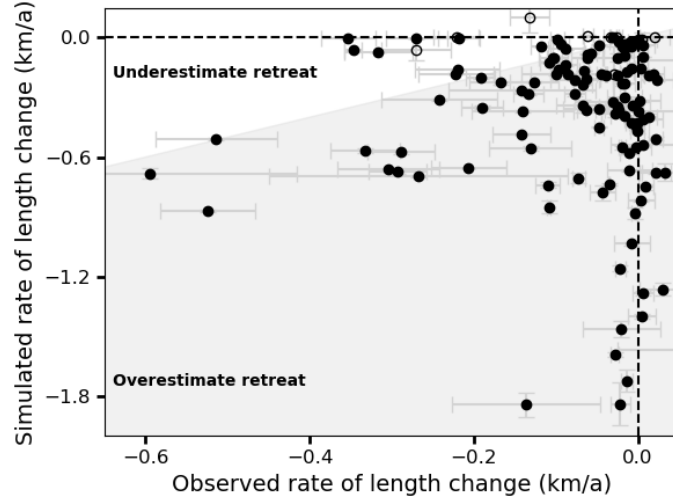
Figure 2. Comparison of observed and simulated rate of retreat for all glaciers simulated. Markers indicate the slope of linear fits to the observed (x-axis) and simulated (y-axis) terminus positions over the 2006-2014 period. Error bars indicate the error on each linear regression. Open circles indicate oscillating termini that are not well captured by linear regression to simulated position (p>0.05; $n = 9$).
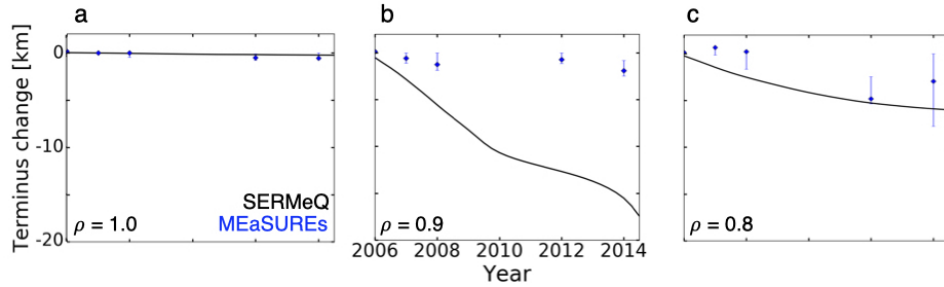

Figure 3. Comparisons of observed and simulated terminus position change for (a) Apuseeq Anittangasikkaajuk (glacier ID 137), where SERMeQ underestimates the true rate of retreat; (b) Helheim Glacier (glacier ID 175), where SERMeQ overestimates retreat; (c) Sermeq Kujalleq (glacier ID 3), where SERMeQ captures observed retreat. Black curves indicate SERMeQ-simulated terminus positions, while blue markers indicate MEaSUREs observations. The blue lines show the most-advanced and most-retreated parts of the terminus projected onto the centerline, and blue diamonds indicate the centroid of the observed terminus projected onto the centerline. Lower left corner annotations give Spearman's rank correlation coefficient ρ between observed and simulated terminus position change for each glacier. Plots share both x- and y-axis scales.
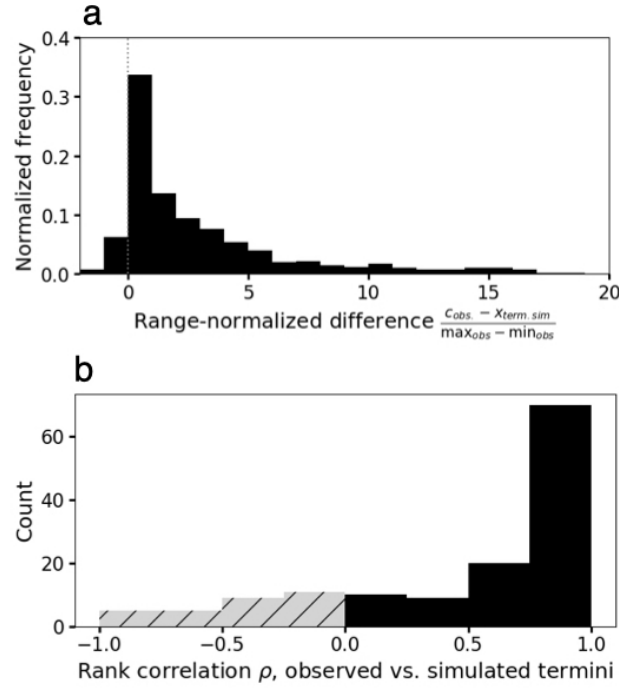
Figure 4. Histograms of (a) Range-normalized difference in terminus position, where the simulated terminus position $x_{\text{term.sim.}}$ is compared with the centroid of the observed terminus c_{obs} and normalized by the range of observed terminus positions (max_{obs} - min_{obs}) along the flowline in the same year; and (b) Spearman's rank-correlation coefficient, ρ, between observed and simulated terminus positions for all glaciers.

3.2 Upper bound retreat rates are realistic

A useful upper bound on calving retreat would consistently overestimate the rate of retreat (Figure 2), simulate terminus positions relatively close to observed termini, and correlate with observed changes. We quantify SERMeQ's performance on the latter indicators in Figure 4.

The histogram in Figure 4a summarizes 404 comparisons of simulated versus observed terminus positions, normalized by each glacier's observational range for each year, such that values within ± 1 indicate simulated terminus positions within the observed range. 40% of simulated terminus positions fall within that range, and 55% of simulated terminus positions are within twice the range of the observed—that is, the simulations are relatively close to the observations. Most simulated terminus positions are more retreated than the observed (positive x-axis values in Figure 4), as expected for an upper bound.

Because we present an upper bound on retreat rather than a calibrated model fit, we do not expect a linear relationship between simulated and observed retreat. Instead, we assess Spearman's rank correlation coefficient for each glacier's terminus positions over time. The coefficient ρ ranges from -1 to 1, where positive ρ indicates that retreat is observed when the model simulates retreat, advance is observed when the model simulates advance, and larger magnitudes of observed and simulated change correspond. Of the 155 glaciers we simulate, ρ is positive for 103, as shown in Figure 4b. For 62 glaciers simulated, $\rho \geq 0.5$ and significant at the $p < 0.1$ level, which indicates a moderately strong and statistically significant relationship between simulated and observed terminus position over time. Only 2 glaciers have negative ρ significant at the same level. The mean ρ over all 155 glaciers is 0.5.

4 Discussion

Our simulated upper-bound rate of terminus retreat/advance emerges as a dynamic glacier response to climate forcing and glacier geometry (Equation 1) and does not rely on any tuning to match observations. The two model parameters, yield strength of glacier ice τ_y and ice temperature T, are physical quantities constrained by laboratory and field observations, and neither is optimized against observed retreat rates. The yield strengths we use for most Greenland outlet glaciers simulated here range from 50-250 kPa (Supplementary Text S3), well within the range of 50-500 kPa suggested by previous works (Nimmo, 2004; O'Neel et al., 2005; Cuffey & Paterson, 2010). We use an ice temperature of $-10°C$, which is also within the range expected from simple physical scaling (van der Veen, 2013), observations (Clow et al., 1996), and modeling (Greuell & Konzelmann, 1994). It is possible an improved match to observed retreat rates could be found if we did allow parameters to vary within and between glacier catchments or over time. However, that would sacrifice the physical upper bound in favor of empirical tuning that cannot be independently constrained by laboratory or field observations.

The upper-bound retreat rate computed from Equation 1 can far exceed the observed rate, as shown in Figures 2 and 3b. There are three notable sources of discrepancy between the modelled and observed retreat rates shown in Figures 2-4: (1) quality of available model input data, (2) performance of automated flowline selection algorithm, and (3) presence of floating ice. First, on small outlets that are rarely visited or studied in detail, the bed topography and climate reanalysis data used as input for SERMeQ may be poorly constrained. As a result, the simulated glacier evolves in response to conditions that do not accurately reflect the local environment, and the simulated change in terminus position is more likely to be inaccurate. Second, on small or slow-moving outlets, or where there are gaps in Sentinel-1 velocity data, our method for tracing flowlines (Text S5) is prone to error. As a result, the simulated glacier has unrealistic geometry

and may flow over bedrock features that are not present in a true central flowline of the outlet. Finally, where floating tongues are present, we remove them and simulate the first grounded grid point as the "terminus". This can change the near-terminus stress state, in some cases exposing an unstable wall of thick ice and initiating rapid retreat. Effects (1) and (2) are likely responsible for the underestimated retreat of Apuseeq Anittangasikkaajuk; effect (3) is likely responsible for the overestimated retreat of Helheim Glacier (see Supplementary Text S6). The first two effects can be mitigated with improved observational data and manual data processing where possible. The third effect reflects upper-bound retreat dynamics that are currently held in check by floating ice, but which we speculate could be activated if that floating ice were removed.

The 91% satisfaction of the intended upper bound on retreat rate (Figure 2) supports the utility of our model for producing upper bounds on calving retreat and dynamic mass loss. In contrast to existing estimates of 21st-century calving loss, our approach does not impose a uniform calving rate or outlet glacier speedup factor (Pfeffer et al., 2008; Graversen et al., 2011; Goelzer et al., 2013; DeConto & Pollard, 2016; Goelzer et al., 2020, accepted); instead, we calculate a theoretical maximum rate of calving retreat that can vary by glacier (Bassis & Ultee, 2019). The result is a physically consistent bound on terminus position change that correlates with observed changes for most glaciers (Figure 4b). By contrast, simpler bounding methods such as imposing a fixed minimum terminus position would have no relationship ($\rho = 0$) with observed terminus position change. Further, our model can track terminus retreat and mass loss from multiple interacting branches of a glacier tributary network (Ultee & Bassis, 2017; Ultee, 2018), ensuring that potentially important contributions to sea level are not overlooked. Within ice-sheet-scale models, our method could be implemented as a calving criterion at grounded ice-ocean interface cells or used as a module to enhance resolution of outlet glacier networks.

The current version of SERMeQ does not explicitly simulate frontal ablation by submarine melting, which can be a large component of mass loss from both floating tongues and grounded glacier fronts (Rignot et al., 2010; Enderlin & Howat, 2013; Wood et al., 2018). Our derivation of Equation 1, which we emphasise is an upper bound on retreat rate, is consistent with high submarine melt that prevents the glacier terminus from advancing (see Supplementary Text S4 and Ma, 2018; Ma & Bassis, 2019). However, changes in ocean conditions over time can affect glacier terminus dynamics such that the rate of terminus position change becomes closer to or farther from the theoretical maximum. For example, a decrease in submarine melt rate has been implicated in the recent slowing of Sermeq Kujalleq's retreat (Khazendar et al., 2019). Future implementations of our method in larger-scale models may therefore benefit from modifications to account for time-varying submarine melt rates.

5 Conclusions

We have applied a flowline network model of ice dynamics, SERMeQ, to evaluate an upper bound on annual to decadal-scale calving retreat of 155 Greenland outlet glaciers in response to variable climate forcing. Comparison with nearly a decade of terminus position records from MEaSUREs (Joughin et al., 2015, updated 2017a) shows that the model bounds retreat rate for 91% of glaciers examined, and that 55% of simulated terminus positions are within twice the observed range. SERMeQ can also evolve upstream surface elevation with each change in terminus position and compute the resultant loss of ice mass above buoyancy (Supplementary Text S1; Ultee, 2018). The upper bound on retreat rate that we construct with SERMeQ will produce a corresponding high-end estimate of the loss of grounded ice mass, consistent with efforts to find an upper bound on the ice-dynamics contribution to 21st century sea level rise. Our approach is especially promising in constraining the dynamic sea level contribution from smaller outlet glaciers that are difficult to resolve in larger-scale continental ice sheet models.

References

Albrecht, T., & Levermann, A. (2012). Fracture field for large-scale ice dynamics. *Journal of Glaciology*, *58*(207), 165–176. doi: 10.3189/2012JoG11J191

Aschwanden, A., Fahnestock, M. A., & Truffer, M. (2016). Complex Greenland outlet glacier flow captured. *Nature Communications*, *7*, 10524 EP. doi: 10.1038/ncomms10524

Aschwanden, A., Fahnestock, M. A., Truffer, M., Brinkerhoff, D. J., Hock, R., Khroulev, C., . . . Khan, S. A. (2019). Contribution of the Greenland Ice Sheet to sea level over the next millennium. *Science Advances*, *5*(6). doi: 10.1126/sciadv.aav9396

Bassis, J. N., & Ultee, L. (2019). A thin film viscoplastic theory for calving glaciers: Towards a bound on the calving rate of glaciers. *Journal of Geophysical Research: Earth Surface*, *124*. doi: 10.1029/2019JF005160

Bassis, J. N., & Walker, C. C. (2012). Upper and lower limits on the stability of calving glaciers from the yield strength envelope of ice. *Proceedings of the Royal Society of London A: Mathematical, Physical and Engineering Sciences*, *468*(2140), 913–931. doi: 10.1098/rspa.2011.0422

Beckmann, J., Perrette, M., & Ganopolski, A. (2018). Simple models for the simulation of submarine melt for a Greenland glacial system model. *The Cryosphere*, *12*(1), 301–323. doi: 10.5194/tc-12-301-2018

Benn, D. I., Åström, J., Zwinger, T., Todd, J., Nick, F. M., Cook, S., . . . Luckman, A. (2017). Melt-under-cutting and buoyancy-driven calving from tidewater glaciers: new insights from discrete element and continuum model simulations. *Journal of Glaciology*, *63*(240), 691-702. doi: 10.1017/jog.2017.41

Benn, D. I., Cowton, T., Todd, J., & Luckman, A. (2017). Glacier calving in Greenland. *Current Climate Change Reports*, *3*(4), 282–290. doi: 10.1007/s40641-017-0070-1

Borstad, C. P., Khazendar, A., Larour, E., Morlighem, M., Rignot, E., Schodlok, M. P., & Seroussi, H. (2012). A damage mechanics assessment of the Larsen B ice shelf prior to collapse: Toward a physically-based calving law. *Geophysical Research Letters*, *39*(18), L18502. doi: 10.1029/2012GL053317

Brown, C. S., Meier, M. F., & Post, A. (1982). *Calving speed of Alaska tidewater glaciers, with application to Columbia Glacier* (Tech. Rep. No. Geological Survey Professional Paper 1258-C). US Government Printing Office.

Catania, G. A., Stearns, L. A., Sutherland, D. A., Fried, M. J., Bartholomaus, T. C., Morlighem, M., . . . Nash, J. (2018). Geometric controls on tidewater glacier retreat in central western Greenland. *Journal of Geophysical Research: Earth Surface*, *123*(8), 2024-2038. doi: 10.1029/2017JF004499

Choi, Y., Morlighem, M., Rignot, E., Mouginot, J., & Wood, M. (2017, 2019/12/18). Modeling the response of Nioghalvfjerdsfjorden and Zachariae Isstrøm glaciers,

Greenland, to ocean forcing over the next century. *Geophysical Research Letters*, *44*(21), 11,071–11,079. doi: 10.1002/2017GL075174

Clow, G. D., Saltus, R. W., & Waddington, E. D. (1996). A new high-precision borehole-temperature logging system used at GISP2, Greenland, and Taylor Dome, Antarctica. *Journal of Glaciology*, *42*(142), 576-584. doi: 10.3189/S0022143000003555

Cuffey, K., & Paterson, W. (2010). *The physics of glaciers* (4th ed.). Elsevier Science, Burlington, MA and Kidlington, United Kingdom. Retrieved from `https://books.google.com/books?id=Jca2v1u1EKEC`

DeConto, R. M., & Pollard, D. (2016). Contribution of Antarctica to past and future sea-level rise. *Nature*, *531*, 591 EP. doi: 10.1038/nature17145

Duddu, R., Bassis, J. N., & Waisman, H. (2013). A numerical investigation of surface crevasse propagation in glaciers using nonlocal continuum damage mechanics. *Geophysical Research Letters*, *40*(12), 3064–3068. doi: 10.1002/grl.50602

Emetc, V., Tregoning, P., Morlighem, M., Borstad, C., & Sambridge, M. (2018). A statistical fracture model for Antarctic ice shelves and glaciers. *The Cryosphere*, *12*(10), 3187–3213. doi: 10.5194/tc-12-3187-2018

Enderlin, E. M., & Howat, I. M. (2013). Submarine melt rate estimates for floating termini of Greenland outlet glaciers (2000–2010). *Journal of Glaciology*, *59*(213), 67–75. doi: 10.3189/2013JoG12J04967

Enderlin, E. M., Howat, I. M., Jeong, S., Noh, M.-J., van Angelen, J. H., & van den Broeke, M. R. (2014). An improved mass budget for the Greenland ice sheet. *Geophysical Research Letters*, *41*(3), 866–872. doi: 10.1002/2013GL059010

Enderlin, E. M., O'Neel, S., Bartholomaus, T. C., & Joughin, I. (2018). Evolving environmental and geometric controls on Columbia Glacier's continued retreat. *Journal of Geophysical Research: Earth Surface*, *123*, 1528 - 1545. doi: 10.1029/2017JF004541

ENVEO. (2017). *Greenland ice velocity map 2016/2017 from Sentinel-1 [version 1.0].* `http://products.esa-icesheets-cci.org/products/details/greenland_ice_velocity_map_winter_2016_2017_v1_0.zip/`.

Felikson, D., Bartholomaus, T. C., Catania, G. A., Korsgaard, N. J., Kjær, K. H., Morlighem, M., ... Nash, J. D. (2017). Inland thinning on the Greenland ice sheet controlled by outlet glacier geometry. *Nature Geoscience*, *10*(5), 366–369. doi: 10.1038/ngeo2934

Goelzer, H., Huybrechts, P., Fürst, J. J., Nick, F. M., Andersen, M. L., Edwards, T. L., ... Shannon, S. (2013). Sensitivity of Greenland Ice Sheet projections to model formulations. *Journal of Glaciology*, *59*(216), 733-749. doi: 10.3189/2013JoG12J182

Goelzer, H., Nowicki, S., Payne, A., Larour, E., Seroussi, H., Lipscomb, W. H., ... van den Broeke, M. (2020, accepted). The future sea-level contribution of the greenland ice sheet: a multi-model ensemble study of ismip6. *The Cryosphere Discussions*, 1–43. doi: 10.5194/tc-2019-319

Graversen, R. G., Drijfhout, S., Hazeleger, W., van de Wal, R., Bintanja, R., & Helsen, M. (2011). Greenland's contribution to global sea-level rise by the end of the 21st century. *Climate Dynamics*, *37*(7), 1427–1442. doi: 10.1007/s00382-010-0918-8

Greuell, W., & Konzelmann, T. (1994). Numerical modelling of the energy balance and the englacial temperature of the Greenland Ice Sheet. Calculations for the ETH-Camp location (West Greenland, 1155 m a.s.l.). *Global and Planetary Change*, *9*(1), 91–114. doi: 10.1016/0921-8181(94)90010-8

Greve, R. (2000). On the response of the Greenland Ice Sheet to greenhouse climate change. *Climatic Change*, *46*(3), 289–303. doi: 10.1023/A:1005647226590

Hanson, B., & Hooke, R. L. (2000). Glacier calving: a numerical model of forces in the calving-speed/water-depth relation. *Journal of Glaciology*, *46*(153), 188-

196. doi: 10.3189/172756500781832792

Joughin, I., Smith, B., Howat, I. M., & Scambos, T. (2015, updated 2017a). *MEa-SUREs Annual Greenland Outlet Glacier Terminus Positions from SAR Mosaics, Version 1.* NASA National Snow and Ice Data Center Distributed Active Archive Center. Boulder, Colorado USA. doi: https://doi.org/10.5067/DC0MLBOCL3EL

Joughin, I., Smith, B., Howat, I. M., & Scambos, T. (2015, updated 2017b). *MEa-SUREs Greenland Ice Sheet Velocity Map from InSAR Data, Version 2.* NASA National Snow and Ice Data Center Distributed Active Archive Center. Boulder, Colorado USA. doi: https://doi.org/10.5067/OC7B04ZM9G6Q

Joughin, I., Smith, B., Howat, I. M., Scambos, T., & Moon, T. (2010). Greenland flow variability from ice-sheet-wide velocity mapping. *Journal of Glaciology*, *56*(197), 415-430. doi: 10.3189/002214310792447734

Khan, S. A., Kjær, K. H., Bevis, M., Bamber, J. L., Wahr, J., Kjeldsen, K. K., . . . Muresan, I. S. (2014). Sustained mass loss of the northeast Greenland ice sheet triggered by regional warming. *Nature Climate Change*, *4*, 292 EP. doi: 10.1038/nclimate2161

Khazendar, A., Fenty, I. G., Carroll, D., Gardner, A., Lee, C. M., Fukumori, I., . . . Willis, J. (2019). Interruption of two decades of Jakobshavn Isbrae acceleration and thinning as regional ocean cools. *Nature Geoscience*, *12*(4), 277–283. doi: 10.1038/s41561-019-0329-3

Krug, J., Weiss, J., Gagliardini, O., & Durand, G. (2014). Combining damage and fracture mechanics to model calving. *The Cryosphere*, *8*(6), 2101–2117. doi: 10.5194/tc-8-2101-2014

Levermann, A., Albrecht, T., Winkelmann, R., Martin, M. A., Haseloff, M., & Joughin, I. (2012). Kinematic first-order calving law implies potential for abrupt ice-shelf retreat. *The Cryosphere*, *6*(2), 273–286. doi: 10.5194/tc-6-273-2012

Lucas-Picher, P., Wulff-Nielsen, M., Christensen, J. H., Aalgeirsdóttir, G., Mottram, R., & Simonsen, S. B. (2012). Very high resolution regional climate model simulations over Greenland: Identifying added value. *Journal of Geophysical Research: Atmospheres*, *117*(D2). doi: 10.1029/2011JD016267

Ma, Y. (2018). *Calving behavior of tidewater glaciers* (Doctoral dissertation, University of Michigan). Retrieved from https://deepblue.lib.umich.edu/handle/2027.42/146058

Ma, Y., & Bassis, J. N. (2019). The effect of submarine melting on calving from marine terminating glaciers. *Journal of Geophysical Research: Earth Surface*, *124*(2), 334–346. doi: 10.1029/2018JF004820

Maussion, F., Butenko, A., Champollion, N., Dusch, M., Eis, J., Fourteau, K., . . . Marzeion, B. (2019). The open global glacier model (OGGM) v1.1. *Geoscientific Model Development*, *12*(3), 909–931. doi: 10.5194/gmd-12-909-2019

Meier, M. F., & Post, A. (1987). Fast tidewater glaciers. *Journal of Geophysical Research: Solid Earth*, *92*(B9), 9051–9058. Retrieved from http://dx.doi.org/10.1029/JB092iB09p09051 doi: 10.1029/JB092iB09p09051

Mercenier, R., Lüthi, M. P., & Vieli, A. (2019). A transient coupled ice flow-damage model to simulate iceberg calving from tidewater outlet glaciers. *Journal of Advances in Modeling Earth Systems*. doi: 10.1029/2018MS001567

Morlighem, M., Bondzio, J., Seroussi, H., Rignot, E., Larour, E., Humbert, A., & Rebuffi, S. (2016). Modeling of Store Gletscher's calving dynamics, West Greenland, in response to ocean thermal forcing. *Geophysical Research Letters*, *43*(6), 2659–2666. doi: 10.1002/2016GL067695

Morlighem, M., Williams, C. N., Rignot, E., An, L., Arndt, J. E., Bamber, J. L., . . . Zinglersen, K. B. (2017). BedMachine v3: Complete bed topography and ocean bathymetry mapping of Greenland from multibeam echo sounding combined with mass conservation. *Geophysical Research Letters*, *44*(21), 11,051-11,061.

doi: 10.1002/2017GL074954

Morlighem, M., Wood, M., Seroussi, H., Choi, Y., & Rignot, E. (2019). Modeling the response of northwest Greenland to enhanced ocean thermal forcing and subglacial discharge. *The Cryosphere*, *13*(2), 723–734. doi: 10.5194/tc-13-723-2019

Mottram, R., Boberg, F., & Langen, P. (2018). *Greenland surface mass balance from Regional Climate Model HIRHAM5.* http://prudence.dmi.dk/data/temp/RUM/HIRHAM/GREENLAND/. Danish Meteorological Institute, Copenhagen, DK.

Mottram, R., Nielsen, K. P., Gleeson, E., & Yang, X. (2017). Modelling glaciers in the HARMONIE-AROME NWP model. *Advances in Science and Research*, *14*, 323–334. doi: 10.5194/asr-14-323-2017

Nick, F. M., Vieli, A., Andersen, M. L., Joughin, I., Payne, A., Edwards, T. L., ... van de Wal, R. S. W. (2013). Future sea-level rise from Greenland's main outlet glaciers in a warming climate. *Nature*, *497*(7448), 235–238. doi: 10.1038/nature12068

Nimmo, F. (2004). What is the Young's modulus of ice? In *Europa's icy shell.*

Noël, B., van de Berg, W. J., van Wessem, J. M., van Meijgaard, E., van As, D., Lenaerts, J. T. M., ... van den Broeke, M. R. (2018). Modelling the climate and surface mass balance of polar ice sheets using RACMO2 – Part 1: Greenland (1958–2016). *The Cryosphere*, *12*(3), 811–831. doi: 10.5194/tc-12-811-2018

Nye, J. F. (1951). The flow of glaciers and ice-sheets as a problem in plasticity. *Proceedings of the Royal Society of London A: Mathematical, Physical and Engineering Sciences*, *207*(1091), 554–572. doi: 10.1098/rspa.1951.0140

O'Neel, S., Pfeffer, W. T., Krimmel, R., & Meier, M. (2005). Evolving force balance at Columbia Glacier, Alaska, during its rapid retreat. *Journal of Geophysical Research: Earth Surface*, *110*(F3), F03012. doi: 10.1029/2005JF000292

Pfeffer, W. T., Harper, J. T., & O'Neel, S. (2008). Kinematic constraints on glacier contributions to 21st-century sea-level rise. *Science*, *321*(5894), 1340–1343. doi: 10.1126/science.1159099

Pollard, D., DeConto, R. M., & Alley, R. B. (2015). Potential Antarctic Ice Sheet retreat driven by hydrofracturing and ice cliff failure. *Earth and Planetary Science Letters*, *412*, 112 - 121. doi: 10.1016/j.epsl.2014.12.035

Price, S. F., Lipscomb, W., Hoffman, M., Hagdorn, M., Rutt, I., Payne, T., ... Kennedy, J. H. (2015). *CISM 2.0.5 Documentation.* http://oceans11.lanl.gov/trac/CISM/data/cism_documentation_v2.0.pdf.

Price, S. F., Payne, A. J., Howat, I. M., & Smith, B. E. (2011). Committed sea-level rise for the next century from Greenland ice sheet dynamics during the past decade. *Proceedings of the National Academy of Sciences*, *108*(22), 8978–8983. doi: 10.1073/pnas.1017313108

Rae, J. G. L., Aalgeirsdóttir, G., Edwards, T. L., Fettweis, X., Gregory, J. M., Hewitt, H. T., ... van den Broeke, M. R. (2012). Greenland ice sheet surface mass balance: evaluating simulations and making projections with regional climate models. *The Cryosphere*, *6*(6), 1275–1294. doi: 10.5194/tc-6-1275-2012

Rignot, E., Koppes, M., & Velicogna, I. (2010). Rapid submarine melting of the calving faces of West Greenland glaciers. *Nature Geoscience*, *3*, 187 EP. doi: 10.1038/ngeo765

Solgaard, A. M., Simonsen, S. B., Grinsted, A., Mottram, R., Karlsson, N. B., Hansen, K., ... Sørensen, L. S. (2020). Hagen Bræ: A surging glacier in North Greenland—35 years of observations. *Geophysical Research Letters*, *47*(6), e2019GL085802. doi: 10.1029/2019GL085802

Sun, S., Cornford, S. L., Moore, J. C., Gladstone, R., & Zhao, L. (2017). Ice shelf fracture parameterization in an ice sheet model. *The Cryosphere*, *11*(6), 2543–2554. doi: 10.5194/tc-11-2543-2017

Sutherland, D. A., Jackson, R. H., Kienholz, C., Amundson, J. M., Dryer, W. P., Duncan, D., . . . Nash, J. D. (2019). Direct observations of submarine melt and subsurface geometry at a tidewater glacier. *Science*, *365*(6451), 369–374. doi: 10.1126/science.aax3528

Ultee, L. (2018). *Constraints on the dynamic contribution to 21st-century sea level rise from Greenland outlet glaciers* (Doctoral dissertation, University of Michigan). Retrieved from `https://deepblue.lib.umich.edu/handle/2027.42/145794`

Ultee, L., & Bassis, J. N. (2016). The future is Nye: An extension of the perfect plastic approximation to tidewater glaciers. *Journal of Glaciology*, *62*(236), 1143-1152. doi: 10.1017/jog.2016.108

Ultee, L., & Bassis, J. N. (2017). A plastic network approach to model calving glacier advance and retreat. *Frontiers in Earth Science*, *5*(24). doi: 10.3389/feart.2017.00024

van den Broeke, M. R., Box, J., Fettweis, X., Hanna, E., Noël, B., Tedesco, M., . . . van Kampenhout, L. (2017). Greenland Ice Sheet surface mass loss: Recent developments in observation and modeling. *Current Climate Change Reports*, *3*(4), 345–356. doi: 10.1007/s40641-017-0084-8

van den Broeke, M. R., Enderlin, E. M., Howat, I. M., Kuipers Munneke, P., Noël, B. P. Y., van de Berg, W. J., . . . Wouters, B. (2016). On the recent contribution of the Greenland ice sheet to sea level change. *The Cryosphere*, *10*(5), 1933–1946. doi: 10.5194/tc-10-1933-2016

van der Veen, C. (2013). *Fundamentals of glacier dynamics* (2nd ed.). Boca Raton, FL, USA: Taylor & Francis.

Winkelmann, R., Martin, M. A., Haseloff, M., Albrecht, T., Bueler, E., Khroulev, C., & Levermann, A. (2011). The Potsdam Parallel Ice Sheet Model (PISM-PIK) – Part 1: Model description. *The Cryosphere*, *5*(3), 715–726. doi: 10.5194/tc-5-715-2011

Wood, M., Rignot, E., Fenty, I., Menemenlis, D., Millan, R., Morlighem, M., . . . Seroussi, H. (2018). Ocean-induced melt triggers glacier retreat in northwest Greenland. *Geophysical Research Letters*, *45*(16), 8334–8342. doi: 10.1029/2018GL078024

Supporting Information for
"SERMeQ model produces realistic retreat of 155 Greenland outlet glaciers"

Lizz Ultee[1]and Jeremy Bassis[2]

[1]Department of Earth, Atmospheric, and Planetary Sciences, Massachusetts Institute of Technology, Cambridge, MA, USA.
[2]Department of Climate & Space Sciences, University of Michigan, Ann Arbor, MI, USA.

Contents

Additional Supporting Information (Files uploaded separately)

1. Table S1, a list of all Greenland outlet glaciers in the MEaSUREs dataset with their glacier ID number, name(s), optimal yield strength found, and notes on inclusion in the analysis. The note "Flagged for bad flowline trace" indicates glaciers that required manual intervention to complete data processing, but which are now included in the analysis.

Introduction

Text S1. Ice dynamics in SERMeQ

The ice dynamics in our model are based on a perfectly-plastic limiting case of a viscoplastic rheology (Bassis & Ultee, 2019). This rheology describes a glacier with two characteristic timescales: viscous deformation (slow) and mass loss by calving (fast). Modifications to the simple plastic formulation allow calving at a grounded ice-water interface (Ultee & Bassis, 2016) and interaction between multiple tributary glaciers (Ultee & Bassis, 2017). By requiring instantaneous stress balance across the glacier terminus, this formulation finds that the ice thickness H_{terminus} at a given terminus position, in water of depth D, is limited by the yield strength and cannot exceed the yield thickness,

$$H_{\text{y}} = 2\frac{\tau_{\text{y}}}{\rho_{\text{i}}g} + \sqrt{\frac{\rho_{\text{w}}}{\rho_{\text{i}}}D^2 + 2\frac{\tau_{\text{y}}}{\rho_{\text{i}}g}}, \tag{S1}$$

with τ_{y} the yield strength of glacier ice, $\rho_{\text{i}} = 920$ kg m^{-3} the density of glacier ice, $\rho_{\text{w}} = 1020$ kg m^{-3} the density of seawater, and $g = 9.81$ m s^{-2} the acceleration due to gravity (Ultee & Bassis, 2016).

In a perfectly plastic glacier (Nye, 1951), the upstream ice thickness H along a central flowline, with along-flow direction x and ice surface elevation s, is also controlled by the yield strength:

$$H\frac{\partial s}{\partial x} = \frac{\tau_{\text{y}}}{\rho_{\text{i}}g}. \tag{S2}$$

This approximation corresponds to a case where the glacier bed is (nearly) plastic and the glacier stress balance is dominated by shear at the glacier bed and valley walls—appropriate for most Greenland outlet glaciers. We also account for longitudinal

---

Corresponding author: L. Ultee, `ehultee@umich.edu`

stresses in a boundary layer near the terminus, where they are more likely to be important (Bassis & Ultee, 2019).

Finally, we use mass continuity to derive an expression for the rate of terminus advance or retreat due to calving (see Text S2, below). With each change in terminus position, we calculate a new surface profile according to Equations S1-S2, and we integrate the changes in ice volume above buoyancy throughout the catchment to deduce a contribution to global mean sea level. Figure S1 shows an example sequence of glacier profiles and corresponding sea level contribution as calculated by SERMeQ.
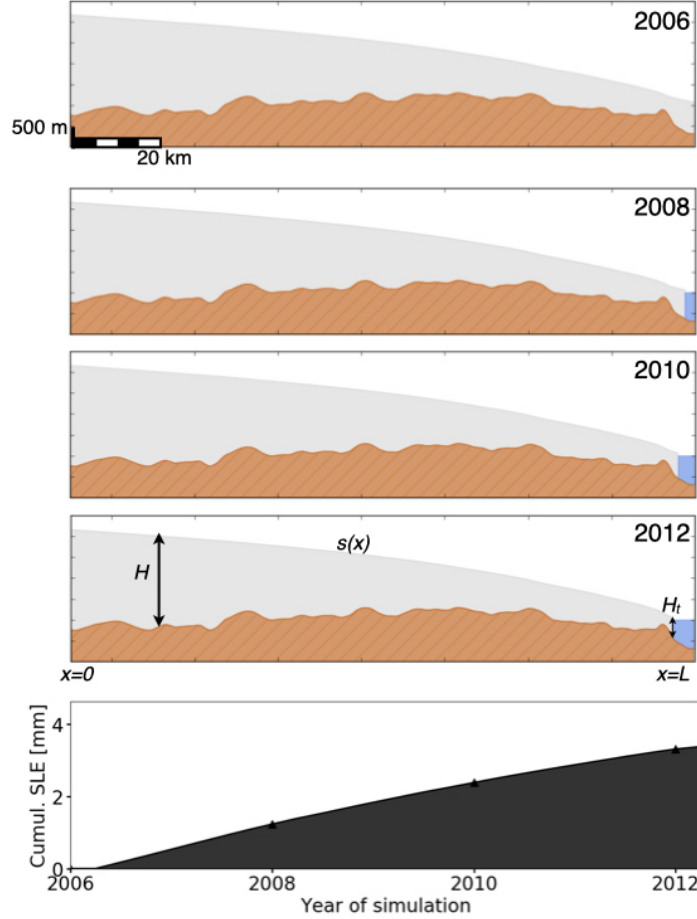

Figure S1. Surface profiles produced by SERMeQ along a flowline in the central part of Sermeq Kujalleq's catchment, with corresponding cumulative sea level contribution (SLE) below. Profiles show glacier ice in grey, bedrock in brown, and fjord water in blue. Spatial scale is indicated on the 2006 panel and consistent throughout. Labels on 2012 panel indicate along-flow direction x, ice surface elevation $s(x)$, ice thickness H, terminus ice thickness H_t, and terminus location $x=L$ as used in Equations S1-S6. Cumulative SLE on bottom panel reflects catchment-integrated loss of ice volume above buoyancy converted to an equivalent volume of seawater and distributed over the area of the global ocean.

Despite the simplicity of the model, preliminary experiments have shown promise in reproducing both surface elevation profiles and advance/retreat rates of glaciers in Alaska and Greenland (Ultee & Bassis, 2016, 2017). However, our model only applies to grounded glaciers and cannot simulate the dynamics of floating ice tongues or shelves.

Text S2. Time evolution of the terminus position

Glacier terminus position in SERMeQ evolves in response to near-terminus stretching, bedrock topography, and changes in catchment-wide surface mass balance as described in Ultee (2018) and Bassis and Ultee (2019). Below is a brief summary derivation of the terminus evolution condition as implemented in SERMeQ code.

Let $x = 0$ represent the ice divide and $x = L$ the terminus, where $L = L(t)$ is the length of the glacier (labelled in Figure S1). The time derivative dL/dt then represents the change in terminus position over time.

Taking the material derivative of the terminus ice thickness $H = H_\mathrm{y}$ (constrained by Equation S1), we find

$$\left.\frac{DH}{Dt}\right|_{x=L} = \frac{DH_\mathrm{y}}{Dt}$$
$$\left[\frac{\partial H}{\partial t} + \frac{dL}{dt}\frac{\partial H}{\partial x}\right]_{x=L} = \frac{\partial H_\mathrm{y}}{\partial t} + \frac{dL}{dt}\frac{\partial H_\mathrm{y}}{\partial x}$$
$$\left.\frac{\partial H}{\partial t}\right|_{x=L} = \frac{dL}{dt}\left[\frac{\partial H_\mathrm{y}}{\partial x} - \frac{\partial H}{\partial x}\right]_{x=L} . \tag{S3}$$

Mass continuity requires

$$\frac{\partial H}{\partial t} + \frac{\partial}{\partial x}(HU) = \dot{a} \tag{S4}$$

where $H = H(x,t)$ is the ice thickness, $U = U(x,t)$ the ice velocity, and $\dot{a} = \dot{a}(x,t)$ the net ice accumulation rate, for all (x,t).

Substituting equation (S4) into (S3), we find

$$\dot{a} - H\frac{\partial U}{\partial x} - U\frac{\partial H}{\partial x} = \frac{dL}{dt}\left[\frac{\partial H_\mathrm{y}}{\partial x} - \frac{\partial H}{\partial x}\right]_{x=L} \tag{S5}$$

$$\frac{dL}{dt} = \frac{\dot{a} - H\frac{\partial U}{\partial x} - U\frac{\partial H}{\partial x}}{\frac{\partial H_\mathrm{y}}{\partial x} - \frac{\partial H}{\partial x}} , \tag{S6}$$

with all terms of equation (S6) evaluated at $x = L$, the terminus of the glacier (compare with Equation 54 of Bassis and Ultee (2019)). With the exception of ice accumulation rate $\dot{a}$, all terms are determined by the rheology of ice.

Upstream from the terminus, we assume a plastic yielding layer at the bed of the glacier. A perfectly plastic glacier would have a rigid ice plug above the yielding layer, but the perfect plastic approximation is a limiting case of several other rheologies that could be used to describe the slow deformation of ice in a pseudo-plug (e.g. Balmforth et al., 2006). Here we choose to describe the slow deformation of intact ice with the familiar Glen's flow law. At the terminus, as in Ultee and Bassis (2016, 2017), we require a vertical yield surface to describe the more rapid motion of fractured, disarticulated ice as it calves away from the intact glacier. This implies that the effective stress in a region of length δ upstream from the terminus is within ϵ of the yield strength τ_y. Near the terminus, we have

$$\frac{\partial U}{\partial x} = \dot{\varepsilon}_{xx} = A\tau_{xx}^n$$
$$= A\tau_\mathrm{y}^n, \tag{S7}$$

where flow law exponent $n = 3$ and A is the flow rate parameter of Glen's flow law.

We integrate equation (S4) in x to find

$$\int_0^L \frac{\partial H}{\partial t}\ \mathrm{d}x + (HU)|_{x=L} = \int_0^L \dot{a}\ \mathrm{d}x \tag{S8}$$

$$U(x=L) = \frac{1}{H_{\mathrm{terminus}}} \int_0^L \left[\dot{a} - \frac{\partial H}{\partial t} \right]\ \mathrm{d}x, \tag{S9}$$

and by the chain rule $\frac{\partial H}{\partial t} = \frac{\partial H}{\partial L}\frac{dL}{dt}$. Separating the integral in equation (S9) and expanding $\frac{\partial H}{\partial t}$ gives

$$U(x=L) = \frac{\dot{\alpha}L}{H_{\mathrm{terminus}}} - \frac{dL}{dt}\frac{1}{H_{\mathrm{terminus}}} \int_0^L \frac{\partial H}{\partial L}\ \mathrm{d}x, \tag{S10}$$

where $\dot{\alpha} = \frac{1}{L}\int_0^L \dot{a}\mathrm{d}x$ is the spatially-averaged ice accumulation rate along the flowline.

We now substitute our expressions (S7, S10) in to equation (S4) and rearrange to find

$$\frac{dL}{dt} = \frac{\dot{a} - A\tau_{\mathrm{y}}^3 H_{\mathrm{terminus}} + \frac{\dot{\alpha}L}{H_{\mathrm{terminus}}}\frac{\partial H}{\partial x}}{\frac{\partial H_{\mathrm{y}}}{\partial x} - \frac{\partial H}{\partial x}\left(1 - \frac{1}{H_{\mathrm{terminus}}}\int_0^L \frac{\partial H}{\partial L}\right)}. \tag{S11}$$

We implement a discretized version of Equation S11 to describe the time evolution of glacier terminus position in SERMeQ.

Text S3. The role of adjustable parameters

Yield strength $\tau_{\mathbf{y}}$

For each glacier, we optimize the yield strength τ_y to find the best fit between a reconstructed and observed centerline surface elevation profile. Glaciers with flatter surface slopes, including those close to flotation, are best fit by lower values of τ_{y}. Steeper surface slopes are better fit by higher values of the yield strength. The optimization procedure is discussed in more detail in Ultee and Bassis (2016). The optimal value of τ_{y} found for each glacier is listed in Supplementary Table 1. There is no correlation between optimal yield strength and glacier latitude, and no other spatial pattern is evident.

Figure S2 shows a histogram of the best-fit values of τ_{y} obtained for the Greenland outlets we simulated. A central peak in the distribution shows that approximately 1/3 of the glaciers we simulate have an optimal yield strength between 125 kPa and 150 kPa. A smaller peak shows that there are also several glaciers in our set best fit by yield strengths between 5 kPa-25 kPa.

In this work, we have used a single value of τ_{y} at both the ice-bed interface and the calving front. It is plausible that the ice-bed interface could be deforming more readily than the pure ice at the calving front, for example if the glacier bed is composed of saturated marine sediments or if the ice is very close to flotation. Such a case would lead to low ice surface slopes and a low optimal value of τ_{y}, even though pure ice throughout the glacier may be stronger. We discuss the case of $\tau_{\mathrm{bed}} < \tau_{\mathrm{ice}}$ in Bassis and Ultee (2019).

Ice temperature T

The ice temperature T is used to select an appropriate value of the flow-rate parameter A in Glen's flow law. Here, we use an ice temperature constant in space and time and do not optimize for its value. In our previous work, we have found that warmer ice ($T = -2°$ C) is softer and more prone to rapid retreat. Conversely, colder ice ($T = -30°$ C) is stiffer and retreats more slowly. For more details, we refer the interested reader to Ultee (2018).
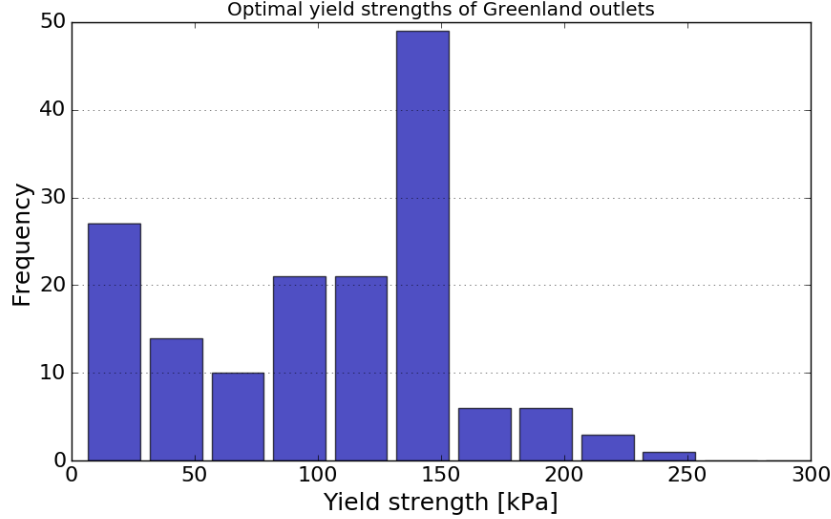
Figure S2. Histogram of optimal yield strength value found for each glacier.

Text S4. Inclusion of submarine melt

We do not explicitly simulate loss of ice from glacier termini by submarine melting. Rather, we have constructed an upper-bound estimate of retreat that is consistent with high submarine melt rates. Our requirement that effective stress near the glacier terminus must equal the yield strength of ice (see Text S1) makes an implicit constraint on the submarine melt rate, because the rate of submarine melt shapes the stress field near glacier termini (Ma, 2018; Ma & Bassis, 2019). There are three cases to consider:

Case I The submarine melt rate is very small compared with the terminus velocity, $u_s \ll u_t$. In this case, the terminus would be able to advance and thin episodically. However, advance and thinning would lower the effective stress at the glacier terminus, such that it would fall below the yield strength of ice and no longer satisfy our criterion. We therefore disallow Case I.

Case II The submarine melt rate is comparable to the terminus velocity, $u_s \sim u_t$. In this case submarine melt would balance the tendency of ice near the terminus to stretch and thin, maintaining the terminus ice thickness at the yield thickness.

Case III The submarine melt rate is very large compared with the terminus velocity, $u_s \gg u_t$. In this case, the erosion of the terminus by high submarine melt would create an overhang and promote calving (Ma & Bassis, 2019). Considered at long enough time scales, e.g. the 0.25 annum standard time step in SERMeQ rather than the hours to days considered in finer-scale process models, high submarine melting and enhanced calving would also maintain the terminus ice thickness at the yield thickness.

Both Cases II and III are consistent with our assumption that there is a yielding boundary layer at the glacier front that constrains the terminus ice thickness (see Bassis & Ultee, 2019). The maximum rate of length change computed in Equation 1 is compatible with both cases, and the ice mass lost in each time step can be considered a combination of mass lost to calving and to submarine melting.

The upper-bound retreat rate that we have sought in this work does not require explicit simulation of the submarine melt rate. Nevertheless, future adaptations of

Figure S3. Network of flowlines on Kangerlussuaq Glacier, MEaSUREs Glacier ID 153, as defined with our tracing and filtering algorithm.

our method to simulate calving in larger-scale models may seek to add a mechanism for forcing by time-varying submarine melt. We suggest that those efforts begin by allowing submarine melt rate u_s to modify the terminus velocity, U in Equation 1, with the understanding that doing so may introduce scenarios that are incompatible with our original assumptions.

Text S5. Flowline network selection

We apply our depth-integrated, width-averaged model on a network of interacting glacier flowlines, as described in Ultee and Bassis (2017). Previous applications have used flowlines selected by hand (Ultee & Bassis, 2016; Ultee, 2018) or by an automated method that detects valley walls of mountain glacier networks (Kienholz et al., 2014; Ultee & Bassis, 2017). Neither method is suitable for the hundreds of Greenland outlet glaciers we consider here. It is impractical to select hundreds of flowlines by hand, and outlets of the Greenland Ice Sheet, unlike mountain glaciers, expand to a nearly featureless catchment upstream with no valley walls to aid in flowline selection. We therefore apply a new selection algorithm based on tracing ice surface velocity.

We begin with a surface velocity composite covering the entire ice sheet (ENVEO, 2017). For each glacier included in the MEaSUREs dataset (Joughin et al., 2015, updated 2017), we extract all points observed along the 2006 terminus position. We then trace each point up the surface velocity field until a pre-determined minimum velocity cutoff (identical for all glaciers); our viscoplastic approximation is most suitable near the glacier terminus (Ultee & Bassis, 2017; Bassis & Ultee, 2019), so we do not extend our simulated catchments all the way to the ice divide. Finally, we filter the set of full-length flowlines so that the most central flowline is defined as the "main trunk". The parallel portions of the remaining flowlines are trimmed and network intersections defined where the angle between flowlines exceeds a threshold value (identical for all glaciers). The code used in network selection is available in our public GitHub repository, and an example network is shown in Figure S3.

The tracing and filtering of flowlines from surface velocity is prone to error where the velocity dataset is noisy or includes holes. Errors in flowline tracing generally become apparent in later data-processing steps, for example if no optimal yield strength

value can be found. Networks affected by such errors include the note "Flagged for bad flowline trace" in Table S1.

Text S6. Detailed case studies

As described in the main article text, 40% of terminus positions simulated by SERMeQ fall within the range of observed terminus position for the same year. Because SERMeQ is sensitive to bed topography features (Ultee, 2018) and is forced by climate reanalysis data, model performance will generally be best where those data products are most accurate. The agreement between modelled and observed retreat of Sermeq Kujalleq (glacier ID 3, also called Jakobshavn Isbræ, main text Figure 3c), where bed topography has been especially well examined by previous glaciological studies, illustrates this point.

It is our aim to produce an upper bound on outlet glacier retreat and associated mass loss. We demonstrated in Bassis and Ultee (2019) that Equation 1 is a theoretical bound on the rate of calving retreat. Thus, we anticipate that the rate of retreat simulated by SERMeQ will generally exceed the observed rate of retreat. To support future implementation of this calving-rate bound in our model or others, it is important to understand where it does not perform as expected. There are two cases to consider: (1) the retreat rate simulated by SERMeQ is slower than the rate observed, or (2) the retreat rate simulated by SERMeQ far exceeds the rate observed (by a factor of 5 or more). We describe three illustrative examples here.

Mean simulated retreat slower than observed

Main text Figure 3a shows the simulated and observed changes in length for Apuseeq Anittangasikkaajuk (MEaSUREs Glacier ID 137), a small outlet glacier on the east coast of Greenland. Our analysis shows that the mean rate of simulated (single point) terminus retreat was 31 m/a, while the mean observed rate of retreat of the terminus centroid was 87 m/a. This is one of only a handful of cases in which the mean observed rate over the 2006-2014 period exceeds the supposed upper-bound rate produced by Equation 1. However, in this case both rates are small, and the simulated terminus position remains within the observed range of terminus positions. We also note that Apuseeq Anittangasikkaajuk is seldom included in other studies of Greenland outlets; as such, the quality of bed topography and climate data for this outlet may be relatively lower.

Mean simulated rate far exceeds observed

Main text Figure 3b shows the simulated and observed changes in length for Helheim Glacier (MEaSUREs Glacier ID 175), a large and well-studied outlet in southeast Greenland. The data quality for this outlet should be comparatively high. Nevertheless, SERMeQ simulates a mean retreat rate of 1980 m/a, which far exceeds the mean observed retreat rate of 313 m/a. We attribute this rapid retreat to features in the bed topography, combined with the no-flotation condition we have implemented in SERMeQ.

The terminus of Helheim Glacier has been observed to float in some years, and was likely floating at the beginning of our simulation period according to bed and surface topography from Morlighem et al. (2017). The glacier bed is more than 600 m below sea level and retrograde for several kilometers upstream of the present terminus, as shown in Figure S4. As explained in main text section 2 and in Ultee and Bassis (2016, 2017), SERMeQ does not allow floating ice tongues to form. Where small tongues are present, we remove them and simulate the first grounded point as the "terminus". In the case of Helheim Glacier, when we removed floating ice, the
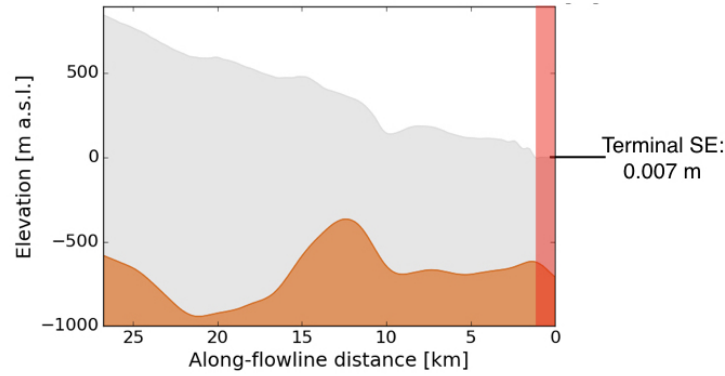
Figure S4. Near-terminus bed topography of Helheim Glacier. Brown filled region shows glacier bed and grey filled region shows glacier ice, both from Morlighem et al. (2017). Note 10:1 exaggeration in vertical scale. A red overlay indicates floating ice that was removed in our simulation. Annotation at figure left indicates the ice surface elevation at the terminus as recorded in Morlighem et al. (2017), further evidence that the initial terminus could not have been grounded ice.

simulated terminus was pushed onto the retrograde bed, where it began an unstable retreat. In summary, the true near-terminus dynamics and stress field of Helheim Glacier are shaped by the presence of floating ice that interacts with the fjord walls. SERMeQ does not include these dynamics and therefore simulates an upper-bound retreat that could occur in the absence of floating ice.

Successive under- and over-estimates within observed period

In a handful of other cases, the rate of retreat observed during a short period exceeds the rate simulated during the same period. Underestimated retreat in one time period is nearly always coupled with overestimated retreat in another period, such that the aggregate effect over the course of the simulation remains an upper-bound estimate of net retreat. For example, between 2007 and 2008, the floating ice tongue of Hagen Brae (MEaSUREs Glacier ID 105) disintegrated (Solgaard et al., 2020). The resulting observed rate of retreat, more than 10 km/a, far exceeded the rate simulated by SERMeQ (< 1 km/a) over the same period (Figure S4). However, our model initialization had already removed the floating portion of the glacier as of 2006, so the SERMeQ-simulated terminus position was still more retreated than the observed. In the subsequent period between 2008 and 2012, SERMeQ slightly overestimated the observed retreat rate. Figure S5 illustrates this history. In Figure S6, we have annotated the floating ice removed upon initialization, the collapse of which was responsible for anomalously high observed retreat between 2007 and 2008.

References

Balmforth, N. J., Craster, R. V., Rust, A. C., & Sassi, R. (2006). Viscoplastic flow over an inclined surface. *Journal of Non-Newtonian Fluid Mechanics*, *139*(1–2), 103 - 127. doi: 10.1016/j.jnnfm.2006.07.010

Bassis, J. N., & Ultee, L. (2019). A thin film viscoplastic theory for calving glaciers: Towards a bound on the calving rate of glaciers. *Journal of Geophysical Research: Earth Surface*, *124*. doi: 10.1029/2019JF005160
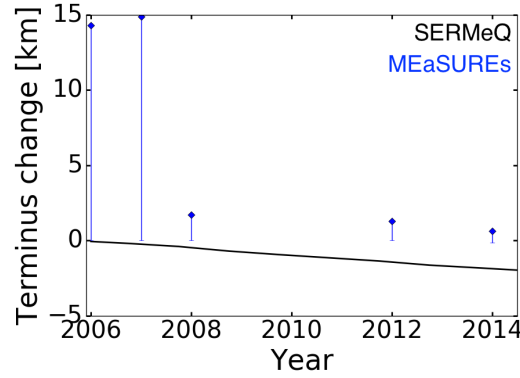
Figure S5. Observed and simulated change in terminus position on Hagen Brae (glacier ID 105). Black curves indicate SERMeQ-simulated terminus positions, while blue markers indicate MEaSUREs observations. The blue lines show the most-advanced and most-retreated parts of the terminus projected onto the centerline, and blue diamonds indicate the centroid of the observed terminus projected onto the centerline. Positive y-axis values indicate terminus positions more advanced than the initial position; negative y-axis values indicate terminus positions retreated from the initial position.
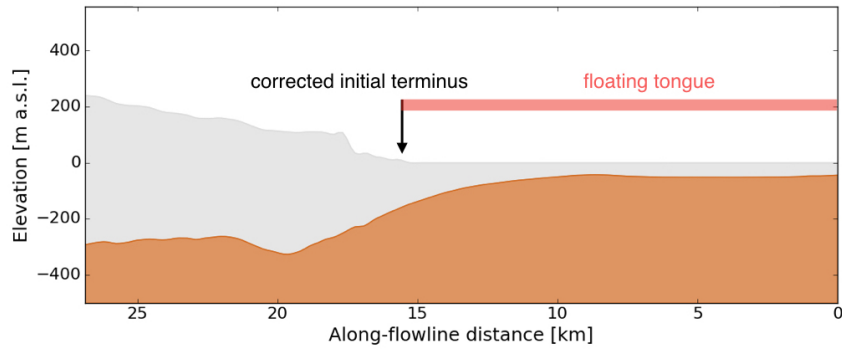

Figure S6. Near-terminus bed topography of Hagen Brae (glacier ID 105). Brown filled region shows glacier bed and grey filled region shows glacier ice, both from Morlighem et al. (2017). Note 10:1 exaggeration in vertical scale. A red bar shows the length of floating ice that was removed during our model initialization, and a black arrow indicates the first grounded point where SERMeQ could establish an initial terminus.

ENVEO. (2017). *Greenland ice velocity map 2016/2017 from Sentinel-1 [version 1.0].* `http://products.esa-icesheets-cci.org/products/details/greenland`$_i ce_v elocity_m ap_w inter_2 016_2$

Joughin, I., Smith, B., Howat, I. M., & Scambos, T. (2015, updated 2017). *MEaSUREs Annual Greenland Outlet Glacier Terminus Positions from SAR Mosaics, Version 1.* NASA National Snow and Ice Data Center Distributed Active Archive Center. Boulder, Colorado USA. doi: https://doi.org/10.5067/DC0MLBOCL3EL

Kienholz, C., Rich, J. L., Arendt, A. A., & Hock, R. (2014). A new method for deriving glacier centerlines applied to glaciers in Alaska and northwest Canada. *The Cryosphere*, *8*(2), 503–519. doi: 10.5194/tc-8-503-2014

Ma, Y. (2018). *Calving behavior of tidewater glaciers* (Doctoral dissertation, University of Michigan). Retrieved from `https://deepblue.lib.umich.edu/handle/2027.42/146058`

Ma, Y., & Bassis, J. N. (2019). The effect of submarine melting on calving from marine terminating glaciers. *Journal of Geophysical Research: Earth Surface*, *124*(2), 334–346. doi: 10.1029/2018JF004820

Morlighem, M., Williams, C. N., Rignot, E., An, L., Arndt, J. E., Bamber, J. L., . . . Zinglersen, K. B. (2017). BedMachine v3: Complete bed topography and ocean bathymetry mapping of Greenland from multibeam echo sounding combined with mass conservation. *Geophysical Research Letters*, *44*(21), 11,051-11,061. doi: 10.1002/2017GL074954

Nye, J. F. (1951). The flow of glaciers and ice-sheets as a problem in plasticity. *Proceedings of the Royal Society of London A: Mathematical, Physical and Engineering Sciences*, *207*(1091), 554–572. doi: 10.1098/rspa.1951.0140

Solgaard, A. M., Simonsen, S. B., Grinsted, A., Mottram, R., Karlsson, N. B., Hansen, K., . . . Sørensen, L. S. (2020). Hagen Bræ: A surging glacier in North Greenland—35 years of observations. *Geophysical Research Letters*, *47*(6), e2019GL085802. doi: 10.1029/2019GL085802

Ultee, L. (2018). *Constraints on the dynamic contribution to 21st-century sea level rise from Greenland outlet glaciers* (Doctoral dissertation, University of Michigan). Retrieved from `https://deepblue.lib.umich.edu/handle/2027.42/145794`

Ultee, L., & Bassis, J. N. (2016). The future is Nye: An extension of the perfect plastic approximation to tidewater glaciers. *Journal of Glaciology*, *62*(236), 1143-1152. doi: 10.1017/jog.2016.108

Ultee, L., & Bassis, J. N. (2017). A plastic network approach to model calving glacier advance and retreat. *Frontiers in Earth Science*, *5*(24). doi: 10.3389/feart.2017.00024